Published in final edited form as:
J Comp Neurol. 2012 December 1; 520(17): 4013–4031. doi:10.1002/cne.23141.

Altered dendritic distribution of dopamine D2 receptors and reduction in mitochondrial number in parvalbumin-containing interneurons in the medial prefrontal cortex of cannabinoid-1 (CB1) receptor knockout mice

Megan L. Fitzgerald[1], **June Chan**[1], **Kenneth Mackie**[2], **Carl R. Lupica**[3], and **Virginia M. Pickel**[1,*]

[1]Division of Neurobiology, Department of Neurology and Neuroscience, Weill Cornell Medical College, 407 East 61st Street, New York, NY 10065

[2]Department of Psychological & Brain Sciences and the Gill Center, Indiana University, Bloomington, Indiana 47405

[3]Electrophysiology Research Section, Cellular Neurobiology Branch, National Institute on Drug Abuse Intramural Research Program, Baltimore, Maryland 21224

Abstract

The prelimbic prefrontal cortex (PL) is a brain region integral to complex behaviors that are highly influenced by cannabinoids and by dopamine D2 receptor (D2R)-mediated regulation of fast-firing parvalbumin-containing interneurons. We have recently shown that constitutive deletion of the cannabinoid CB1 receptor (CB1R) greatly reduces parvalbumin levels in these neurons. The effects of CB1R deletion on PL parvalbumin interneurons may be ascribed to loss of CB1R-mediated retrograde signaling on mesocortical dopamine transmission, and, in turn, altered expression and/or subcellular distribution of the D2R in the PL. Furthermore, diminished parvalbumin expression could indicate metabolic changes in fast-firing interneurons that may be reflected in changes in mitochondrial density in this population. We therefore comparatively examined electron microscopic dual labeling of the D2R and parvalbumin in CB1 (−/−) and CB1 (+/+) mice to test the hypothesis that absence of the CB1R produces changes in D2R localization and mitochondrial distribution in parvalbumin-containing interneurons of the PL. CB1 (−/−) mice had a significantly lower density of cytoplasmic D2R-immunogold particles in medium parvalbumin-labeled dendrites and a concomitant increase in the density of these particles in small dendrites. These dendrites received both excitatory and inhibitory-type synapses from unlabeled terminals and contained many mitochondria, whose numbers were significantly reduced in the CB1 (−/−) mice. Non-parvalbumin containing dendrites showed no between-group differences in either D2R distribution or mitochondrial number. These results suggest that cannabinoid signaling provides an important determinant of dendritic D2 receptor distribution and mitochondrial availability in fast-spiking interneurons.

Keywords

Prelimbic; fast-firing; antipsychotic; electron microscopy; trafficking; marijuana

[*]Address correspondence to: Dr. Virginia M. Pickel, Division of Neurobiology, Weill Cornell Medical College, 407 East 61st Street, New York, NY 10065, Phone: (646) 962-8275, Fax: (646) 962-0535, vpickel@med.cornell.edu.

Introduction

Physiological activation of the prefrontal cortex (PFC) underlies a variety of functions including working memory, attentional processes, adaptation to stress, and autonomic regulation in the mouse and rat (Amat et al., 2005; Dalley et al., 2004; Ulrich-Lai and Herman, 2009) as well as in primates and humans (Miller and Cohen, 2001; Ulrich-Lai and Herman, 2009). The nature of PFC activation and resultant behavior is determined in part by structural and functional interactions between intracortical circuits and mesocortical dopaminergic afferents. Of critical importance within the local circuit are fast-firing parvalbumin interneurons whose dendrites are targeted by dopaminergic projections from the ventral tegmental area (VTA; Sesack et al., 1998).

Dopamine activation of the dopamine D2 receptor (D2R) increases firing of parvalbumin interneurons in the adult mouse PFC (Tseng and O'Donnell, 2007). The D2R is highly expressed in these parvalbumin-containing interneurons of the PFC, whose dysfunction is implicated in schizophrenia (Fung et al., 2010; Spencer et al., 2003). All typical antipsychotics act as D2R antagonists that may ameliorate psychotic symptoms in part through modulation of neuronal activity in the PFC (Wang and Goldman-Rakic, 2004). Because D2R expression levels and subcellular location are markedly affected by agonist activation and may also be influenced by antagonists (Missale et al., 1998), the antipsychotic effectiveness of D2R antagonists may reflect activation-dependent changes in expression and trafficking of D2Rs. Thus, a deeper comprehension of factors that influence D2R expression and/or location in parvalbumin interneurons of the PFC is of particular interest in regards to understanding the neuronal architecture that may be altered in neuropsychiatric disease.

We have recently reported a decrease in parvalbumin immunoreactivity in interneurons of the PFC in mutant mice lacking the cannabinoid-1 receptor (CB1R) (Fitzgerald et al., 2011). The CB1R is the primary central nervous system mediator of the effects of endocannabinoids as well as Δ^9-tetrahydrocannabinol (Δ^9THC), the main psychoactive constituent of marijuana. CB1 receptors are abundantly expressed in limbic-associated brain regions including the prelimbic PFC (PL), where they are primarily located on axon terminals (Bodor et al., 2005a; Lafourcade et al., 2007).

The decrease in parvalbumin immunoreactivity observed in CB1R knock-out mice may reflect diminished activity of this fast-firing population, as parvalbumin expression is linked to neuronal activity (Cellerino et al., 1992). Decreased neuronal activity and associated cellular metabolism may manifest as a decrease in the number of mitochondria in parvalbumin interneurons. Furthermore, this decrease in parvalbumin in the PFC may in part be due to altered expression and/or trafficking of the D2R in mice lacking the CB1R, as postnatal maturation of cortical parvalbumin interneurons is mediated specifically through dopaminergic activation of the D2R (Porter et al., 1999).

We tested the hypothesis that constitutive deletion of the CB1R may affect either D2R distribution or mitochondrial number preferentially in parvalbumin interneurons of the PFC. To do so, we used dual immuno-electron microscopy with antibodies against parvalbumin and the D2R to quantitatively compare D2R and mitochondrial distributions in the PL of C57/BL6J mice lacking the CB1 receptor with wild-type controls.

Methods

Animals

The animal protocols in this study followed NIH guidelines concerning the Care and Use of Laboratory Animals in Research and were approved by the Animal Care Committee at Weill Cornell Medical College. All efforts were made to minimize suffering and to reduce the number of animals needed for experiments. Adult male wild type (CB1+/+) and CB1 knockout (CB1−/−) mice were bred onto a C57BL/6J genetic background. CB1−/− mice were generated as described by Zimmer *et al.*, 1999. Briefly, mice lacking the CB1R were generated by replacing the CB1 coding sequence, which is confined to a single exon between amino acids 32 and 448, with PGK-neo^r through homologous recombination in embryonic stem cells. The absence of the CB1R in the CB1−/− mice generated has been confirmed through ligand binding studies (Zimmer *et al.*, 1999). Mice used in this study were bred from heterozygote stock, which was refreshed periodically with outbred C57BL6/J mice to protect against inbreeding-induced genetic drift. Genotyping was performed by Charles River (Germantown, MD, USA). The six CB1+/+ and four CB1−/− mice used in this study were littermates from three different litters and were matched according to age (ages ranged from 20 to 32 weeks). CB1−/− and CB1+/+ mice were housed together in common litters of 3–5 mice under a 12 h light/dark cycle. Food and water were available *ad libitum*.

Tissue preparation

All mice were deeply anesthetized with sodium pentobarbital (100 mg/kg, i.p.). For electron microscopic analysis, brain tissue was fixed by vascular perfusion through the left ventricle of the heart with sequential delivery of (1) 5 ml of heparin-saline (1000 U/ml), (2) 30 ml of 3.75% acrolein and 2% paraformaldehyde (PFA) in 0.1 M phosphate buffer (PB; pH 7.4), and (3) 100 ml of 2% PFA in 0.1 M PB. Brains were excised from the cranial cavity and post-fixed in 2% PFA in 0.1M PB for 30 min. For immunofluorescent histochemistry, brain tissue was fixed with (1) 5 ml heparin-saline and (2) 250 ml 4% PFA in 0.1M PB and postfixed in 4% PFA for 2 hours. All brains were then transferred to cold 0.1M PB and cut into 40 μm coronal sections on a Vibratome (Leica, Deerfield, IL). Coronal sections through the PFC were selected at 1.94 mm anterior to Bregma (Paxinos and Franklin, 2001).

Antibody characterization

The parvalbumin protein was identified using a well-characterized commercially available mouse monoclonal antibody (Table 1). Specificity has been determined through Western blot analysis of whole-brain homogenate which yields a single band at the molecular weight of parvalbumin and preadsorption controls which eliminate labeling in Western blots as well as cortical sections (Celio and Heizmann, 1981). This antiserum has been used extensively to immunolabel parvalbumin interneurons in numerous light and electron microscopic studies, and the pattern of neuronal parvalbumin labeling we observed is analogous to that previously reported (Alcántara et al., 1993; Celio and Heizmann, 1981; Kita et al., 1990). Moreover, this parvalbumin antibody has been shown to exclusively label fast-spiking interneurons, further demonstrating antibody selectivity (Zaitsev et al., 2005).

The CB1R was identified using an affinity-purified polyclonal antibody raised in guinea pig against peptide sequences within the C-terminus. The guinea pig CB1R antibody used herein shows no immunoreactivity in CB1−/− cortex (Figure 1). Acrolein-fixed sections through the cortex from wild-type and CB1−/− mice were processed for immunoperoxidase labeling as described below in the protocol for dual immunoperoxidase and immunogold labeling for electron microscopy. Briefly, cortical sections from CB1−/− and wild-type mice were incubated together in guinea pig CB1R antiserum at 1:2000 dilution in tris-buffered saline

(TBS; pH 7.6) containing 0.1% bovine serum albumin (BSA; Sigma-Aldrich, St. Louis, MO) for 24 hours at room temperature followed by an overnight incubation at 4°C. The sections were then washed and processed for immunoperoxidase labeling as described below. Sections were then mounted on subbed slides, dehydrated, and coverslipped for visualization of the peroxidase reaction product using a Nikon (Tokyo, Japan) E800 light microscope equipped with a Micropublisher digital camera (Q Imaging, British Columbia, Canada) interfaced with an Apple G4 computer.

CB1R immunoreactivity was not observed in CB1−/− cortex (Figure 1). This finding is consistent with the lack of CB1R immunoreactivity using the same antiserum in CB1−/− striatum (Lane et al., 2011), and CB1−/− hippocampus (Katona et al., 2006), demonstrating antibody specificity. Furthermore, the basket-like patterns of immunoreactivity observed in our study and lack of co-expression of parvalbumin and the CB1R are in accordance with cortical CB1R labeling observed using a CB1R antibody raised in rabbit (Bodor et al., 2005). This rabbit antibody likewise shows no immunoreactivity in the CB1−/− cortex (Bodor et al., 2005).

The D2R was labeled using an affinity-purified antiserum generated in rabbit against the human D2R long isoform (Brana et al., 1997). This sequence was cloned into a pET30c plasmid (Novagen, Madison, WI), and was confirmed using sequencing. Human embryonic kidney cells transiently transfected with the pcDNA-FLAG-D2L plasmid showed positive immunolabeling for the D2R, confirming antibody selectivity. Western blot of rat brain homogenate resulted in a single band immunolabeled for the D2R at the predicted weight of 50kDa (Pickel et al., 2006). This band was eliminated in a preadsorption control, as was D2R immunolabeling in sections of the rat nucleus accumbens, a brain region with high levels of D2R expression (Pickel et al., 2006). To confirm D2R antibody specificity in the mouse PL, the D2R antibody was incubated at working dilution (1:500) with immunizing peptide at 10 μg/mL in a blocking solution of 0.1% BSA in 0.1M TBS while rocking overnight at 4°C (Figure 2). Vibratome sections through the PL from acrolein-fixed brains for immunoperoxidase and PFA-fixed brains for immunofluorescence were incubated in either this adsorbed antiserum or in anti-D2R antibody (1:500) with 0.1% BSA in 0.1M TBS for 24 hours at room temperature followed by an overnight incubation at 4°C. The acrolein-fixed sections were washed and processed for immunoperoxidase labeling as described below, and imaged as described previously for CB1R immunoperoxidase labeling. The PFA-fixed sections were processed and imaged as described below under triple immunofluorescent labeling and confocal imaging. Identical confocal imaging parameters were used for adsorption control and D2R labeled tissue.

To control for secondary antibody specificity, a mouse brain section was included in each experiment that had been fixed in the same manner as experimental tissue but had not been exposed to primary antiserum. No specific immunoperoxidase, immunogold, or immunofluorescent labeling was evident in this tissue (data not shown).

Triple immunofluorescent labeling and confocal imaging

Tissue was rinsed in 0.05 M phosphate buffered saline (PBS; pH 7.4) prior to blocking in 0.25% Triton (Sigma-Aldrich, St. Louis, MO) with 0.5% BSA and 5% normal goat serum (NGS; Jackson ImmunoResearch, West Grove, PA) in 0.05 M PBS for 2 hours. Brain sections were then washed in 0.05 M PBS prior to overnight incubation at room temperature in the primary antibody cocktail containing 0.1% Triton, 0.5% BSA, and 5% NGS with CB1R (1:2000), D2R (1:500), and parvalbumin (1:3000) primary antisera. Tissue was then rinsed in 0.1% Triton and 5% NGS in PBS for 30 min over multiple washes and rinsed in PBS. Tissue was incubated for 2 hours in 0.1% Triton and 5% NGS in PBS containing secondary antibodies goat anti-guinea pig AlexaFluor488 (1:400; Invitrogen, Carlsbad, CA),

goat anti-rabbit AlexaFluor633 (1:200), and goat anti-mouse AlexaFluor546 (1:400). Brain sections were washed for one hour over multiple rinses in PBS prior to mounting on subbed slides in 0.05M PB, coverslipped with ProLong Gold antifade mounting media (Invitrogen), and sealed with clear nail polish.

Slides were imaged using a Leica TCS SP5 confocal microscope interfaced with LAS AF Version 2.0.2 (Leica Microsystems, ©2005–2008) computer software on a PC computer. Images of individual channels were sequentially captured using a monochrome CCD camera and were pseudocolored using the LAS AF software. Images were digitally collected in a 1024 ×1024 pixel frame using X20, X40, or X63 objective lenses. Images from individual channels and the compilation of all three channels are shown. Adobe Photoshop CS4 (Adobe Systems, Inc.) was used to compile images, crop, adjust brightness and contrast, incorporate symbols and text, and prepare figures.

Dual immunoperoxidase and immunogold labeling for electron microscopy

To ensure identical labeling conditions between CB1+/+ and CB1−/− mice, sections through the PFC were marked with identifying punches and pooled for processing. Free-floating brain sections were processed for dual immunoperoxidase and immunogold-silver labeling of parvalbumin and the D2R, respectively (Chan et al., 1990). Sections were placed in 1% sodium borohydride in 0.1 M PB for 30 min and then washed thoroughly in 0.1 M PB. A freeze-thaw cycle was induced to enhance penetration of the immunoreagents. First, sections were incubated in a cryoprotectant solution (25% sucrose and 3.5% glycerol in 0.05M PB) for 15 min then rapidly freeze-thawed by immersion in 1) liquid chlorodifluoromethane (Freon, Refron Inc., NY), 2) liquid nitrogen, and 3) room temperature 0.1 M PB. Sections were then rinsed in 0.1 M TBS.

To block non-specific binding of antisera, sections were incubated in 0.5% BSA in 0.1 M TBS for 30 minutes. Following rinses in 0.1 M TBS, the sections were incubated in the primary antibody solution, which consisted of the mouse anti-parvalbumin (1:3000) and rabbit anti-D2R (1:350) with 0.1% BSA in 0.1 M TBS. Incubation in this primary antibody cocktail occurred over 12 h at room temperature followed by 36 h at 4° C.

Immunoperoxidase labeling was chosen for parvalbumin as a qualitative secondary marker of interneuron soma and processes, while punctate immunogold-silver was chosen as the secondary marker for the D2R to determine quantitative differences in D2R distribution. This combination allows comparison of D2R distribution in two populations of neurons in the PFC (interneurons expressing parvalbumin and neuronal profiles including pyramidal neurons that express the D2R but not parvalbumin).

For immunoperoxidase labeling, sections of tissue were rinsed in 0.1 M TBS following primary antibody incubation. They were then incubated for 30 min in a 1:400 dilution of biotinylated horse anti-mouse immunoglobulin G (IgG) (Jackson ImmunoResearch Laboratories, Inc., West Grove, PA), washed in 0.1 M TBS, and in avidin-biotin peroxidase complex (Vectastain Elite Kit, Vector Laboratories, Burlingame, CA) for 30 min. After thorough rinses with 0.1 M TBS, the peroxidase reaction product was generated in 0.022% 3,3′-diaminobenzidine (DAB, Aldrich, Milwaukee, WI) and 0.003% hydrogen peroxide in 0.1 M TBS for 6 min.

For immunogold-silver labeling, tissue sections were rinsed in 0.01 M phosphate-buffered saline (PBS; pH 7.4) after the DAB reaction, blocked in a solution of 0.8% BSA with 0.1% gelatin in 0.01 M PBS for 10 min and incubated for 2h in a 1:50 dilution of goat anti-rabbit IgG conjugated with one nm colloidal gold (Amersham, Arlington Heights, IL, USA). Sections were then washed with 0.1 M TBS and incubated in 2% glutaraldehyde. Sections

were rinsed in 0.01 M PBS followed by 0.2 M citrate buffer (pH 7.4). Silver-enhancement of the IgG-conjugated gold particles was performed using the IntenS-EM kit (Amersham) for 5 min at room temperature. Sections were rinsed in 0.2 M citrate buffer and 0.1 M PB prior to post-fixation in 2% osmium tetroxide in 0.1 M PB for 1 h. The post-fixed sections were washed in 0.1 M PB followed by dehydration through a graded series of ethanols and propylene oxide. These sections were incubated overnight in a 1:1 mixture of propylene oxide and Epon (Embed 812) (Electron Microscopy Sciences, Fort Washington, PA). Sections were transferred to 100% Epon for 2 h prior to flat-embedding between two sheets of Aclar plastic.

The area containing the PL (Figure 3A) was trimmed into a trapezoid and cut into ultra-thin (65 nm) sections with a diamond knife (Diatome, Fort Washington, PA) on an ultratome (Leica, Deerfield, IL). These ultra-thin sections were collected on a 400-mesh copper grid (Electron Microscopy Sciences) and counterstained with uranyl acetate and lead citrate prior to electron micrograph capture.

Electron Microscopic Analysis

Ultra-thin sections were examined at 60 kV with a Philips CM10 transmission electron microscope (FEI, Hillsboro, OR). Digital images for presentation and analysis were captured using an AMT Advantage HR/HR-B CCD camera (Advantage Microscopy Techniques, Danvers, MA). Images were obtained exclusively from the Epon-tissue interface where there is optimal penetration of primary and secondary antisera.

The electron microscopic images were analyzed by an investigator blind to genotype, using identical sampling methods for all images. For each of the 10 mice, the entire PL was examined from the molecular layer through layer VI. Images for quantification were captured at 19,000X magnification wherever both secondary labels were visible within the same frame (22 μm^2) to ensure that the area quantified was permeable to both immunogold and immunoperoxidase labels. The site of each micrograph was recorded and a total of 825 micrographs were captured (representing 18,150 μm^2 of neuropil area). These 825 micrographs represent the sum total of 22 μm^2 frames within the PL from the 10 animals in the study containing both immunogold D2R and immunoperoxidase parvalbumin labeling. This relatively small amount of micrographs compared to the sample size and area examined reflects the small percentage of parvalbumin interneurons in the mouse PL respective to other neuronal cell types in the region. Furthermore representative of the distribution of parvalbumin interneurons, approximately 17% of micrographs containing parvalbumin-immunoreactive processes were taken from areas corresponding to superficial layers of the PL, 65% from middle layers of the PL, and 18% from deep layers. Micrographs for presentation were prepared using Adobe Photoshop and Microsoft PowerPoint 2008 (Microsoft Corporation) to crop, insert text and symbols, adjust brightness and contrast, and compile figure panels.

Neuronal profiles containing parvalbumin and/or D2R immunoreactivity were identified according to the criteria set forth by Peters, et al (1991). Briefly, axon terminals were characterized by an extensive presence of synaptic vesicles. Axonal processes often but not always contained synaptic vesicles and frequently were observed to be grouped in bundles. Dendritic profiles were identified mainly by their lack of synaptic vesicles and receptivity to inputs from vesicle-filled axon terminals. In addition, dendrites usually contained an abundance of endoplasmic reticulum and mitochondria that were largely absent from dendritic spines. These spines typically showed a thickened post-synaptic membrane specialization beneath a vesicle-filled axon terminal. Labeled profiles that were unable to be unequivocally identified were not included in the analysis. This criterion may have led to an

underrepresentation of dendritic spine neck and small axon counts, as these two profile types were frequently quite difficult to reliably distinguish.

A profile was regarded as positive for the immunoperoxidase labeling when it contained a diffuse electron-dense product not seen in other nearby profiles considered to be unlabeled. Profiles considered immunogold labeled contained two or more gold particles (<~40 nm) or a single large (>~40 nm) particle, since many of the larger particles appeared to be aggregates of smaller particles. However, small dendritic spine profiles less than 0.5 μm in maximum axis diameter were considered immunolabeled if they contained a single gold particle to prevent false negative exclusion of small labeled profiles. Minimal false positive identification of D2R-labeled profiles was ensured by examining the percentage of gold particles overlying myelin, which is not known to contain the D2R, and can therefore serve as a control for spurious immunogold.

D2R immunogold particles were categorized as to whether they were in contact with the plasmalemmal membrane, and/or within a profile containing the parvalbumin immunoperoxidase reaction product. To assure reliable assessment of dual labeling, only profiles whose entirety fit within the frame and were not occluded by grid bars were included in counts and analysis. Therefore, neuronal somata were excluded, as they were too large to fit within a single micrograph.

To ensure that perfusion differences and/or inconsistencies in the level of section imaged did not contribute to between-group differences, total immunogold/area was compared between individual subjects in each group, and was not found to be significantly different (for +/+, $F = 1.27$, $p = 0.28$; for −/−, $F = 0.73$, $p = 0.48$). MCID Elite software (version 6, Imaging Research Inc., Ontario, Canada) was used to measure the cross-sectional diameter, cytoplasmic area, and plasmalemmal perimeter of 2,454 immunolabeled neuronal profiles. From these measurements, the following between-group comparisons were calculated using a student's T-test: 1) average diameter of parvalbumin-labeled dendrites, 2) average diameter of parvalbumin + D2R-labeled dendrites, 3) cytoplasmic density of D2R-immunogold in parvalbumin-labeled dendrites, 4) cytoplasmic density of D2R-immunogold in non parvalbumin-labeled dendrites, 5) average size of D2R-labeled dendritic spines, 6) plasmalemmal D2R-immunogold labeling in parvalbumin-dendrites, 7) plasmalemmal D2R-immunogold in non-parvalbumin dendrites, 8) density of D2R-immunogold in parvalbumin-labeled axon terminals, and 9) density of D2R-immunogold in non-parvalbumin axon terminals. None of these comparisons were found to be statistically significant.

The dendritic shaft, however, is not a homogeneous entity. Larger parvalbumin dendrites are likely to be proximal to the soma, contain extensive endoplasmic reticulum and are more likely than small and medium-sized dendrites to be receptive to symmetric inhibitory-type synaptic contacts. Medium-sized dendrites are often receptive to multiple asymmetric excitatory-type contacts and contain an abundance of mitochondria, multivesicular bodies, and other organelles, whereas small dendrites are likely to be most distal to the soma and are sometimes contiguous with dendritic spines. Therefore, K-means cluster analysis by dendritic diameter was used to statistically divide D2R immunogold labeled dendrites into small, medium, and large categories to compare D2R immunogold distribution between these subgroups using a student's T-test. JMP version 8.0.2 (SAS Institute, Inc.) computer software was used for statistical analysis while Prism Version 5 for Mac OS X (GraphPad Software, Inc.) was used to generate graphs of data.

Results

In the PL of wild-type mice, fluorescent microscopy showed that neuronal processes expressing the CB1R frequently contacted cells containing D2R-like immunoreactivity and less often apposed cells immunolabeled for parvalbumin. Electron microscopic ultrastructural analysis of CB1+/+ and CB1−/− PL revealed D2R immunoreactivity in a few glial and many neuronal profiles, only the latter of which also contained parvalbumin immunoreactivity. The D2R and parvalbumin were observed in many of the same somatodendritic and some of the same axonal profiles in the PL of both CB1+/+ and CB1−/− mice. Overall D2R and parvalbumin immunolabeling patterns in CB1+/+ and CB1−/− mice were similar (Table 2), and did not differ between groups by chi-squared analysis ($\lambda^2 = 7.062$, $p = 0.53$). In mutant mice, however, both the subcellular distribution of D2R-immunogold and the number of mitochondria were selectively altered in dendrites of parvalbumin containing neurons.

Parvalbumin interneurons frequently express the D2R but not the CB1R in the wild-type mouse prelimbic PFC

Fluorescence microscopy revealed a laminar distribution pattern of cortical CB1R immunoreactivity consistent with past reports (Figure 3B; Bodor et al., 2005a; Lafourcade et al., 2007). This characteristic CB1R labeling highlights dense networks of axonal processes, most prominently in Layers II/III and again in VI. Parvalbumin immunolabeled somata were most prevalent in middle to deeper cortical layers, while D2R immunoreactive cell bodies did not show a layer-specific distribution, suggestive of D2R expression by both interneurons and pyramidal projection neurons of the PL. Most parvalbumin-containing interneurons were immunoreactive for the D2R, and no parvalbumin soma contained the CB1R (Figure 3C–F). Some of the interneurons co-expressing the D2R and parvalbumin were targeted by CB1R labeled axons that formed basket-like patterns of immunoreactivity around the soma (Figure 3F). More frequently, however, CB1R-immunoreactive neuronal processes surrounded D2R-labeled soma that did not contain parvalbumin but were also contacted by parvalbumin-immunoreactive processes (Figure 3G–J).

Ultrastructural somatic D2R and parvalbumin distribution in the prelimbic PFC

Electron microscopic analysis showed that somata immunolabeled for parvalbumin contained many mitochondria and often had invaginated nuclear membranes in both CB1+/+ and CB1−/− mice. Some nuclei of parvalbumin-immunoreactive somata also contained parvalbumin immunoreactivity (Figure 4A), an observation in agreement with findings that this calcium-binding protein is diffusible across neuronal compartments (Schmidt et al., 2007). Within parvalbumin-labeled somata, D2R immunogold was often distributed along patches of endomembrane and on the plasmalemmal surface (Figure 4A, B). Consistent with our previous report (Fitzgerald et al., 2011), somatic parvalbumin labeling appeared more sparsely distributed in CB1−/− mice (Figure 4A, B). The synaptic inputs to somata containing parvalbumin frequently included axon terminals forming asymmetric excitatory-type synapses, and occasionally terminals forming symmetric inhibitory-type synapses. Glial processes were also often in apposition to parvalbumin-immunoreactive somata. Most somata containing the D2R but not parvalbumin bore many characteristics of pyramidal projection neurons, including stacked Golgi apparatuses (Figure 4C) and prominent apical dendrites (Peters et al., 1991). These somata were frequently contacted by parvalbumin-labeled terminals that formed symmetric inhibitory-type axosomatic synapses (Figure 4C).

Pre- and post-synaptic D2R and parvalbumin distribution in the prelimbic PFC

Dendrites singly-labeled for parvalbumin or the D2R as well as dually-labeled dendrites were observed (Figure 5). Dendritic shafts containing parvalbumin often received multiple

asymmetric-type inputs onto the dendritic shaft (Figure 5A, B). In both CB1+/+ and CB1−/− mice, 75% of the clearly defined presynaptic terminals onto parvalbumin-immunolabeled dendritic profiles formed asymmetric excitatory-type synapses, while 25% formed symmetric inhibitory-type contacts. However, dendritic profiles singly-labeled for the D2R received fewer inputs from inhibitory-type terminals in CB1−/− mice relative to CB1+/+ controls (Figure 5C; see also Figure 7A). This trend was driven by a decrease in parvalbumin-positive axon terminals presynaptic to D2R-labeled dendrites in the CB1−/− PL. In CB1+/+ mice, 33 of 68 (49%) of recognizable synapses on D2R-labeled dendritic shafts were symmetric, while in $CB1^{-/-}$ mice 33 of 87 (39%) of recognizable synapses were symmetric. Of these total symmetric contacts on D2R-immunoreactive segments of the dendritic shaft without visible parvalbumin, 41% expressed parvalbumin in the CB1+/+ PL, while just 21% were parvalbumin-immunolabeled in the CB1−/− PL ($\lambda^2 = 7.16$, df = 1, $p < 0.01$).

Axon terminals containing D2R immunogold more often formed asymmetric compared to symmetric synapses in both the CB1+/+ and CB1−/− PL, and this did not differ between genotypes. These D2R labeled terminals occasionally targeted dendrites of parvalbumin immunoreacitve interneurons (Figure 5B). A small but significant number of presynaptic terminals containing the D2R also were labeled for parvalbumin (Figure 5D), and these terminals exclusively formed symmetric inhibitory-type contacts. In both CB1+/+ and CB1−/− PL, the vast majority (~97%) of discernible synapses formed by axon terminals singly labeled for parvalbumin were symmetric inhibitory-type.

Selectively altered cytoplasmic D2R distribution in parvalbumin-containing dendrites of the prelimbic PFC in CB1 knock-out mice

Dendrites co-expressing the D2R and parvalbumin had diameters ranging from 0.229 to 1.139 μm (n = 187). There was no significant difference in dendritic diameter between groups; nor did statistical variance differ. In small parvalbumin-labeled dendrites of the PL (diameters ranging from 0.229 μm to 0.520 μm, n = 68), there was a significant increase in cytoplasmic D2R immunogold in CB1−/− mice relative to controls ($t_{(66)} = 2.34$, $p < 0.05$ Figure 6A, B, E). In contrast, CB1−/− mice showed a significant decrease in cytoplasmic D2R in medium-sized parvalbumin-labeled dendrites of the PL (diameters ranging from 0.529 μm to 0.764 μm, n = 69; $t_{(67)} = 2.27$, $p < 0.05$; Figure 6C–E). Large parvalbumin-expressing dendrites (n = 50, diameters ranging from 0.796 μm to 1.139 μm) showed no statistically significant ($p < 0.05$) difference in cytoplasmic D2R expression between CB1+/+ and CB1−/− mice. Regardless of dendritic size, plasmalemmal D2R immunogold did not significantly differ between CB1+/+ and CB1−/− mice (Figure 6F).

In the PL, the D2R-containing dendrites in the PL not expressing parvalbumin may belong to pyramidal neurons that differ extensively in size and morphology from interneurons. Therefore, discrete K-means cluster analyses were undertaken to segregate small, medium, and large diameter D2R dendrites in parvalbumin and non-parvalbumin from 0.161 μm to 2.681 μm in diameter (n = 912). In this group, there were no statistically significant between-group differences in cytoplasmic or plasmalemmal D2R immunogold in small (0.161–0.690 μm diameter, n = 665), medium (0.691–1.443 μm diameter, n = 231), and large (1.513–2.681 μm, n = 16) dendritic profiles (Figure 7). Furthermore, there were no statistically significant between-group differences in D2R immunogold labeling of dendritic spines (n = 178, Figure 8).

Reduction in mitochondrial number in parvalbumin-containing dendrites of CB1−/− mice

Mitochondria were counted in dendrites, axons, and axon terminals that were immunolabeled for the D2R, parvalbumin, or both. Significantly fewer mitochondria were

observed in all sizes of parvalbumin-containing dendritic profiles with or without the D2R in CB1−/− mice relative to wild-type controls ($t_{(313)} = 1.98$, $p < 0.05$, Figure 9). There was no significant size difference of parvalbumin-containing dendrites between groups as measured through minimum axis diameter, and variances in dendritic size were statistically equivalent in both groups. No significant between-group differences in mitochondrial number per unit area were observed in dendrites without parvalbumin labeling or in presynaptic (axonal) profiles.

Discussion

Our results provide the first direct evidence that constitutive deletion of the CB1 receptor gene can alter the subcellular distribution of dendritic D2 receptors and reduce the mitochondrial density selectively in parvalbumin-containing interneurons of the adult mouse PL. These adaptations are consistent with our prior demonstration of reduced parvalbumin expression in interneurons of the PFC in CB1−/− mice (Fitzgerald et al., 2011). The major findings are schematically diagrammed in Figure 10. We speculate that the adaptations seen in the PL of CB1−/− mice are developmentally regulated, but directly involved in modulating ongoing activity and behavior in maturity.

Constitutive genetic deletion of the CB1R results in chronic loss of signaling through this receptor throughout ontogeny. Thus, our findings in the adult PL may largely reflect developmental changes that occur at least partially to compensate for loss of endocannabinoid signaling. This is suggested by evidence that the peak expression levels of parvalbumin, the CB1R, and the D2R are concurrent postnatal events (Alcántara et al., 1993; Heng et al., 2011; Schambra et al., 1994). The coincident crest of parvalbumin, CB1R, and D2R expression might indicate the dual requirement for dopamine and cannabinoid modulation of interneuron activity in the maturation of cortical parvalbumin expression during postnatal development. Fewer mitochondria and altered D2R trafficking in parvalbumin interneurons of the PL in CB1 KO mice may therefore represent secondary adaptations of this neuronal population over development as well as a direct loss of CB1R-mediated effects in adulthood.

Mitochondrial reduction in dendrites of parvalbumin interneurons of CB1−/− mice

We have observed selectively fewer mitochondria in dendrites but not axons of parvalbumin interneurons in the PL of CB1−/− mice compared with wild-type mice. Mitochondria are motile cellular organelles involved in ATP balance and calcium buffering. In neurons, the localization of mitochondria is dynamically regulated to meet local energy demands in dendrites and axons (Wang and Schwarz, 2009) while increasing synaptic activity *in vitro* induces mitochondrial recruitment to dendritic but not axonal synaptic sites (Chang et al., 2006). Furthermore, dynamic mitochondrial relocation to dendritic sites is correlated with synaptogenesis in cultured neurons (Li et al., 2004). The comparatively low mitochondrial density in dendrites of parvalbumin interneurons of the adult PL in CB1−/− mice may therefore indicate decreased synaptic activity and/or decreased calcium buffering capacity within these dendrites.

Cholecystokinin (CCK) and GABA-mediated direct and indirect mechanisms may contribute to the overall inhibition of the activity of parvalbumin interneurons in the adult PL. Our infrequent detection of CB1R immunoreactivity in parvalbumin-containing somata or processes in this region is consistent with evidence that the CB1R is found at low levels in pyramidal neurons (Hill et al., 2007) but is mainly localized to cholecystokinin (CCK) immunoreactive axon terminals (Bodor et al., 2005a). CB1R activation on GABAergic axon terminals inhibits presynaptic vesicle release (Bodor et al., 2005b), leading to an overall disinhibitory effect. Genetic deletion of the CB1R, therefore, may increase vesicle release

from axon terminals of CCK interneurons via the abrogation of endocannabinoid function in the PL. In the hippocampus, axon terminals of CCK basket interneurons form functional synapses onto parvalbumin interneurons (Karson et al., 2009). Similarly, we have observed CB1R immunoreactive basket-like processes surrounding parvalbumin-labeled somata in the wild-type PL, indicating that CCK/CB1R axon terminals may inhibit the activity of parvalbumin neurons in the PFC as well as the hippocampus. Loss of CB1R retrograde signaling may therefore directly increase inhibition of parvalbumin interneuron firing, consistent with the morphological indications observed in this study. Alternatively, CCK/CB1R interneurons may indirectly modulate the activity of parvalbumin interneurons. CCK/CB1R GABAergic axon terminals are known to form functional inhibitory contacts with pyramidal neurons in the adult mouse PFC (Markram et al., 2004; Hill et al., 2011). Increased inhibition of pyramidal neurons in CB1−/− mice may decrease firing of local glutamatergic pyramidal axon collaterals onto dendrites of parvalbumin interneurons, acting to indirectly diminish fast-firing interneuron activity.

Since disruption of mitochondrial motility impairs synapse formation (Li et al., 2004), we cannot exclude the alternate possibility that the reduced mitochondrial density observed in parvalbumin immunoreactive dendrites is a cause rather than a consequence of decreased synaptic activity. Similar mitochondrial deficits have been observed under conditions of oxidative stress and are implicated in neurodegenerative disease as well as in schizophrenia (Keating, 2008; Prabakaran et al., 2004). The decrease in parvalbumin reported in the CB1−/− PL (Fitzgerald et al., 2011) may alter calcium buffering capacities in dendrites (Chard et al., 1993), and this may in turn influence mitochondrial trafficking (Billups and Forsythe, 2002). Indeed, these factors may contribute to increased excitotoxicity observed in CB1−/− mice (Marsicano et al., 2003). Further studies are necessary to definitively determine whether the decrease in parvalbumin expression and mitochondrial number in fast-spiking interneuron is an *a priori* insult or a result of altered synaptic activity over development.

Effects of CB1R deletion on axon terminals expressing parvalbumin or the D2R

Fewer parvalbumin-labeled terminals formed identifiable synaptic contacts onto dendrites containing the D2R in CB1−/− compared with wild-type mice. This may reflect a decrease in parvalbumin immunoreactivity below detectible levels in a number of axon terminals in CB1−/− mice (Fitzgerald et al., 2011). Alternatively, the small number of synapses between parvalbumin-labeled terminals and D2R-containing dendrites in CB1−/− mice may be ascribed to less frequent axonal branching in parvalbumin interneurons of CB1−/− mice. This is suggested by the observation that axonal branching is correlated with decreased activity in GABAergic basket interneurons (Chattopadhyaya et al., 2007). Either of these interpretations, however, indicates a functional uncoupling of GABAergic and dopaminergic inputs onto D2R-expressing dendrites, and is likely to affect the output of non-parvalbumin D2R-expressing neurons in CB1−/− mice.

We did not observe presynaptic changes in the distribution of D2R immunoreactivity in symmetric versus asymmetric terminals or in the abundance of D2R immunogold in axon terminals of CB1−/− mice. The D2R antiserum used in this study was generated against amino acids 216–311 in the third cytoplasmic loop of the D2R, which are expressed by the D2 long receptor isoform (D2LR) but not the D2 short receptor isoform (D2SR; Dal Toso et al., 1989; Giros et al., 1989; Kearn et al., 2005). Recent work using an antibody that recognizes an epitope of both the D2LR and the D2SR isoforms has shown extensive CB1R and D2R presynaptic colocalization as well as functional interaction in the PFC (Chiu et al., 2010). The D2LR is most abundant in postsynaptic dendrites but is also presynaptically expressed (Chiu et al., 2010; Wang and Pickel, 2002) whereas the D2SR primarily mediates presynaptic autoreceptor function (Usiello et al., 2000). It is possible therefore that the

D2SR isoform is directly affected by CB1R deletion but we did not detect this change because our antiserum preferentially labels the D2LR.

Selective dendritic D2R trafficking deficit in parvalbumin interneurons of CB1−/− mice

While the D2R is abundantly expressed in both pyramidal neurons and interneurons of the PL (Le Moine and Gasper, 1998; Santana et al., 2008), no changes in D2R expression or distribution were observed in non-parvalbumin containing dendrites in CB1−/− mice. The selective increase in D2R observed in small dendrites and corresponding decrease in D2R immunogold in medium dendritic profiles of parvalbumin interneurons in the PL of CB1 −/− mice may reflect decreased tonic release of dopamine onto these dendrites. The D2R, unlike the D1R, is targeted for lysosomal degradation pathways following activation (Bartlett et al., 2005). Following D2R activation by dopamine, the receptor may be internalized by endocytosis and mobilized through larger dendritic processes towards lysosomal compartments in the soma. In the CB1+/+ mouse, D2R immunogold distribution in parvalbumin interneurons is similar throughout small, medium, and large dendrites, suggesting that the size-dependent variation in D2R-immunogold density in parvalbumin containing dendrites of the CB1−/− mouse PL is a direct reflection of altered dopamine release and/or trafficking of the D2R in these dendrites.

VTA dopaminergic terminals have been shown to contact dendrites of parvalbumin interneurons in the PFC (Sesack et al., 1998) where excitatory actions of dopamine are mediated exclusively through the D2R in the adult rodent cortex (Tseng and O'Donnell, 2007). Midbrain dopaminergic projection neurons rarely express the CB1R but are targeted by GABAergic and glutamatergic axon terminals that abundantly express this receptor (Mátyás et al., 2008). It is accordingly thought that endocannabinoid modulation of the output of VTA dopamine projection neurons follows an indirect path through CB1R activation in presynaptic axon terminals forming synapses onto VTA projection neurons (Lupica et al., 2004). In mice lacking the CB1R, significant reductions in release of dopamine have been observed in microdialysis and voltametric studies as compared to CB1+/+ controls (Li et al., 2009; Soria et al., 2005). Consistent with these observations, CB1R agonist Δ^9THC produces increased dopamine efflux in the mPFC (Chen et al., 1990) as well as an increase in the firing rate of VTA dopaminergic neurons that can be blocked by a CB1R antagonist (French, 1997).

The hypothesis that trafficking deficits observed in CB1 −/− mouse PL are a result of decreased dopamine activation of the D2R in parvalbumin dendrites is substantiated by the observation that postnatal development of parvalbumin expression in the cortex is enhanced by dopamine and is blocked by a D2R but not a D1R antagonist (Porter et al., 1999). Dopamine-mediated maturation of parvalbumin neurons therefore occurs specifically through the D2R and application of a D2R antagonist results in decreased cortical parvalbumin expression that is qualitatively similar to that observed in CB1−/− cortex (Fitzgerald et al., 2011).

Parvalbumin expression is correlated with neuronal activity (Cellerino et al., 1992). Although the D2R is a Gi-coupled receptor and its activation reduces cytosolic cAMP levels and PKA activity as well as firing rates of pyramidal neurons, bath application of the D2R agonist quinpirole specifically enhances the excitability of fast-firing interneurons in the adult rat cortex (Tseng and O'Donnell, 2004). There may therefore be a dichotomous cellular response to decreased dopamine D2R activation in pyramidal neurons and fast-firing interneurons of the PL. This may be reflected in part by the D2R trafficking deficit observed in parvalbumin immunoreactive dendritic profiles but not in profiles without visible parvalbumin immunoreactivity in CB1−/− mice. Ultimately, the combination of dysregulation of distal dopaminergic inputs and local GABAergic and glutamatergic circuits

induced by CB1R deletion may lead to a pronounced deficit of parvalbumin interneurons in the PL.

Acknowledgments

This work was supported by the National Institutes of Health (1PO1 HL096571, MH40342, and DA04600 to VMP; DA011322 and DA021696 to KM; T32 DA 7274 to MLF; and The National Drug Abuse Intramural Research Program, CRL).

References

Alcántara S, Ferrer I, Soriano E. Postnatal development of parvalbumin and calbindin D28K immunoreactivities in the cerebral cortex of the rat. Anat Embryol. 1993; 188:63–73. [PubMed: 8214625]

Amat J, Baratta MV, Paul E, Bland ST, Watkins LR, Maier SF. Medial prefrontal cortex determines how stressor controllability affects behavior and dorsal raphe nucleus. Nature Neuroscience. 2005; 8:365–371.

Bartlett SE, Enquist J, Hopf FW, Lee JH, Gladher F, Kharazia V, Waldhoer M, Mailliard WS, Armstrong R, Bonci A, Whistler JL. Dopamine responsiveness is regulated by targeted sorting of D2 receptors. Proc Natl Acad Sci USA. 2005; 102:11521–11526. [PubMed: 16049099]

Billups B, Forsythe ID. Presynaptic mitochondrial calcium sequestration influences transmission at mammalian central synapses. J Neurosci. 2002; 22:5840–5847. [PubMed: 12122046]

Bodor AL, Katona I, Nyíri G, Mackie K, Ledent C, Hájos N, Freund TF. Endocannabinoid signaling in rat somatosensory cortex: laminar differences and involvement of specific interneuron types. J Neurosci. 2005; 25:6845–6856. [PubMed: 16033894]

Brana C, Aubert I, Charron G, Pellevoisin C, Bloch B. Ontogeny of the striatal neurons expressing the D2 dopamine receptor in humans: an in situ hybridization and receptor-binding study. Brain Res Mol Brain Res. 1997; 48:389–400. [PubMed: 9332736]

Celio MR, Heizmann CW. Calcium-binding protein parvalbumin as a neuronal marker. Nature. 1981; 293:300–302. [PubMed: 7278987]

Cellerino A, Siciliano R, Domenici L, Maffei L. Parvalbumin immunoreactivity: a reliable marker for the effects of monocular deprivation in the rat visual cortex. Neuroscience. 1992; 51:749–753. [PubMed: 1488119]

Chan J, Aoki C, Pickel VM. Optimization of differential immunogold-silver and peroxidase labeling with maintenance of ultrastructure in brain sections before plastic embedding. J Neurosci Methods. 1990; 33:113–127. [PubMed: 1977960]

Chang DTW, Honick AS, Reynolds IJ. Mitochondrial trafficking to synapses in cultured primary cortical neurons. J Neurosci. 2006; 26:7035–7045. [PubMed: 16807333]

Chard PS, Bleakman D, Christakos S, Fullmer CS, Miller RJ. Calcium buffering properties of calbindin D28k and parvalbumin in rat sensory neurones. The Journal of Physiology. 1993; 472:341–357. [PubMed: 8145149]

Chattopadhyaya B, Di Cristo G, Wu CZ, Knott G, Kuhlman S, Fu Y, Palmiter RD, Huang ZJ. GAD67-mediated GABA synthesis and signaling regulate inhibitory synaptic innervation in the visual cortex. Neuron. 2007; 54:889–903. [PubMed: 17582330]

Chen J, Paredes W, Lowinson JH, Gardner EL. Delta 9-tetrahydrocannabinol enhances presynaptic dopamine efflux in medial prefrontal cortex. European Journal of Pharmacology. 1990; 190:259–262. [PubMed: 1963849]

Chiu CQ, Puente N, Grandes P, Castillo PE. Dopaminergic modulation of endocannabinoid-mediated plasticity at GABAergic synapses in the prefrontal cortex. J Neurosci. 2010; 30:7236–7248. [PubMed: 20505090]

Dal Toso R, Sommer B, Ewert M, Herb A, Pritchett DB, Bach A, Shivers BD, Seeburg PH. The dopamine D2 receptor: two molecular forms generated by alternative splicing. EMBO J. 1989; 8:4025–4034. [PubMed: 2531656]

Dalley JW, Cardinal RN, Robbins TW. Prefrontal executive and cognitive functions in rodents: neural and neurochemical substrates. Neuroscience and Biobehavioral Reviews. 2004; 28:771–784. [PubMed: 15555683]

Fitzgerald ML, Lupica CR, Pickel VM. Decreased parvalbumin immunoreactivity in the cortex and striatum of mice lacking the CB1 receptor. Synapse. 2011; 65:827–831. [PubMed: 21445945]

French ED. delta9-Tetrahydrocannabinol excites rat VTA dopamine neurons through activation of cannabinoid CB1 but not opioid receptors. Neuroscience Letters. 1997; 226:159–162. [PubMed: 9175591]

Fung SJ, Webster MJ, Sivagnanasundaram S, Duncan C, Elashoff M, Weickert CS. Expression of interneuron markers in the dorsolateral prefrontal cortex of the developing human and in schizophrenia. The American Journal of Psychiatry. 2010; 167:1479–1488. [PubMed: 21041246]

Giros B, Sokoloff P, Martres MP, Riou JF, Emorine LJ, Schwartz JC. Alternative splicing directs the expression of two D2 dopamine receptor isoforms. Nature. 1989; 342:923–926. [PubMed: 2531847]

Heng L, Beverley JA, Steiner H, Tseng KY. Differential developmental trajectories for CB1 cannabinoid receptor expression in limbic/associative and sensorimotor cortical areas. Synapse. 2011; 65:278–286. [PubMed: 20687106]

Hill EL, Gallopin T, Ferezou I, Cauli B, Rossier J, Schweitzer P, Lambolez B. Functional CB1 receptors are broadly expressed in neocortical GABAergic and glutamatergic neurons. J Neurophysiol. 2007; 97:2580–2589. [PubMed: 17267760]

Hill MN, McLughlin RJ, Pan B, Fitzgerald ML, Roberts CJ, Lee T, Karatsoreos IN, Mackie K, Viau V, Pickel VM, McEwen BS, Liu Q, Gorzalka BB, Hillard CJ. Recruitment of prefrontal cortical endocannabinoid signaling by glucocorticoids contributes to termination of the stress response. J Neurosci. 2011; 31:10506–10515. [PubMed: 21775596]

Karson MA, Tang A-H, Milner TA, Alger BE. Synaptic Cross Talk between Perisomatic-Targeting Interneuron Classes Expressing Cholecystokinin and Parvalbumin in Hippocampus. J Neurosci. 2009; 29:4140–4154. [PubMed: 19339609]

Katona I, Sperlagh B, Sik A, Kafalvi A, Vizi E, Mackie K, Freund T. Presynaptically located CB1 cannabinoid receptors regulate GABA release from axon terminals of specific hippocampal interneurons. J Neurosci. 1999; 19:4544–4558. [PubMed: 10341254]

Katona I, Urbán GM, Wallace M, Ledent C, Jung KM, Piomelli D, Mackie K, Freund TF. Molecular composition of the endocannabinoid system at glutamatergic synapses. J Neurosci. 2006; 26:5628–37. [PubMed: 16723519]

Kearn C, Blake-Palmer K, Daniel E, Mackie K, Glass M. Concurrent stimulation of cannabinoid CB1 and dopamine D2 receptors enhances heterodimer formation: a mechanism for receptor cross-talk? Molecular pharmacology. 2005; 67:1697–1704. [PubMed: 15710746]

Keating DJ. Mitochondrial dysfunction, oxidative stress, regulation of exocytosis and their relevance to neurodegenerative diseases. Journal of Neurochemistry. 2008; 104:298–305. [PubMed: 17961149]

Kita H, Kosaka T, Heizmann CW. Parvalbumin-immunoreactive neurons in the rat neostriatum: a light and electron microscopic study. Brain Research. 1990; 536:1–15. [PubMed: 2085740]

Lafourcade M, Elezgarai I, Mato S, Bakiri Y, Grandes P, Manzoni OJ. Molecular components and functions of the endocannabinoid system in mouse prefrontal cortex. PLoS ONE. 2007; 2:e709. [PubMed: 17684555]

Lane DA, Chan J, Fitzgerald ML, Kearn CS, Mackie K, Pickel VM. Quinpirole elicits differential in vivo changes in the pre- and postsynaptic distributions of dopamine D2 receptors in mouse striatum: Relation to cannabinoid-1 (CB1) receptor targeting. Molecular Psychopharmacology. In press.

Le Moine C, Gaspar P. Subpopulations of cortical GABAergic interneurons differ by their expression of D1 and D2 dopamine receptor subtypes. Molecular Brain Research. 1998; 58:231–236. [PubMed: 9685656]

Li X, Hoffman AF, Peng X-Q, Lupica CR, Gardner EL, Xi Z-X. Attenuation of basal and cocaine-enhanced locomotion and nucleus accumbens dopamine in cannabinoid CB1-receptor-knockout mice. Psychopharmacology. 2009; 204:1–11. [PubMed: 19099297]

Li Z, Okamoto K-I, Hayashi Y, Sheng M. The importance of dendritic mitochondria in the morphogenesis and plasticity of spines and synapses. Cell. 2004; 119:873–887. [PubMed: 15607982]

Lupica CR, Riegel AC, Hoffman AF. Marijuana and cannabinoid regulation of brain reward circuits. British Journal of Pharmacology. 2004; 143:227–234. [PubMed: 15313883]

Markram H, Toledo-Rodriguez M, Wang Y, Gupta A, Silberberg G, Wu C. Interneurons of the neocortical inhibitory system. Nature Reviews Neuroscience. 2004; 5:793–807.

Marsicano G, Goodenough S, Monory K, Hermann H, Eder M, Cannich A, Azad SC, Cascio MG, Gutiérrez SO, van der Stelt M, López-Rodriguez ML, Casanova E, Schütz G, Zieglgänsberger W, Di Marzo V, Behl C, Lutz B. CB1 cannabinoid receptors and on-demand defense against excitotoxicity. Science. 2003; 302:84–88. [PubMed: 14526074]

Mátyás F, Urbán GM, Watanabe M, Mackie K, Zimmer A, Freund TF, Katona I. Identification of the sites of 2-arachidonoylglycerol synthesis and action imply retrograde endocannabinoid signaling at both GABAergic and glutamatergic synapses in the ventral tegmental area. Neuropharmacology. 2008; 54:95–107. [PubMed: 17655884]

Miller EK, Cohen JD. An integrative theory of prefrontal cortex function. Annu Rev Neurosci. 2001; 24:167–202. [PubMed: 11283309]

Missale C, Nash SR, Robinson SW, Jaber M, Caron MG. Dopamine receptors: from structure to function. Physiol Rev. 1998; 78:189–225. [PubMed: 9457173]

Paxinos, G.; Franklin, KBJ. The Mouse Brain in Stereotaxic Coordinates. Academic Press; San Diego, CA: 2001.

Peters, A.; Palay, SL.; Webster, HD. The Fine Structure of the Nervous System. Oxford University Press, Inc; New York, NY: 1991.

Pickel VM, Chan J, Kearn CS, Mackie K. Targeting dopamine D2 and cannabinoid-1 (CB1) receptors in rat nucleus accumbens. The Journal of Comparative Neurology. 2006; 495:299–313. [PubMed: 16440297]

Porter LL, Rizzo E, Hornung JP. Dopamine affects parvalbumin expression during cortical development in vitro. J Neurosci. 1999; 19:8990–9003. [PubMed: 10516317]

Prabakaran S, Swatton JE, Ryan MM, Huffaker SJ, Huang JT-J, Griffin JL, Wayland M, Freeman T, Dudbridge F, Lilley KS, Karp NA, Hester S, Tkachev D, Mimmack ML, Yolken RH, Webster MJ, Torrey EF, Bahn S. Mitochondrial dysfunction in schizophrenia: evidence for compromised brain metabolism and oxidative stress. Mol Psychiatry. 2004; 9:684697, 643.

Santana N, Mengod G, Artigas F. Quantitative analysis of the expression of dopamine D1 and D2 receptors in pyramidal and GABAergic neurons of the rat prefrontal cortex. Cerebral Cortex. 2009; 19:849–860. [PubMed: 18689859]

Schambra B, Duncan G, Breese G, Fornaretto M, Caron M, Fremeau R. Ontogeny of D-1A and D-2 Dopamine-Receptor subtypes in rat brain using in-situ hybridization and receptor-binding. Neuroscience. 1994; 62:65–85. [PubMed: 7816213]

Schmidt H, Arendt O, Brown EB, Schwaller B, Eilers J. Parvalbumin is freely mobile in axons, somata and nuclei of cerebellar Purkinje neurones. Journal of neurochemistry. 2007; 100:727–35. [PubMed: 17263794]

Sesack SR, Hawrylak VA, Melchitzky DS, Lewis DA. Dopamine innervation of a subclass of local circuit neurons in monkey prefrontal cortex: ultrastructural analysis of tyrosine hydroxylase and parvalbumin immunoreactive structures. Cereb Cortex. 1998; 8:614–622. [PubMed: 9823482]

Soria G, Mendizábal V, Touriño C, Robledo P, Ledent C, Parmentier M, Maldonado R, Valverde O. Lack of CB1 cannabinoid receptor impairs cocaine self-administration. Neuropsychopharmacology. 2005; 30:1670–1680. [PubMed: 15742004]

Spencer KM, Nestor PG, Niznikiewicz MA, Salisbury DF, Shenton ME, McCarley RW. Abnormal neural synchrony in schizophrenia. J Neurosci. 2003; 23:7407–7411. [PubMed: 12917376]

Tseng K-Y, O'Donnell P. Dopamine modulation of prefrontal cortical interneurons changes during adolescence. Cereb Cortex. 2007; 17:1235–1240. [PubMed: 16818475]

Tseng KY, O'Donnell P. Dopamine-glutamate interactions controlling prefrontal cortical pyramidal cell excitability involve multiple signaling mechanisms. J Neurosci. 2004; 24:5131. [PubMed: 15175382]

Ulrich-Lai YM, Herman JP. Neural regulation of endocrine and autonomic stress responses. Nature Reviews Neuroscience. 2009; 10:397–409.

Usiello A, Baik JH, Rougé-Pont F, Picetti R, Dierich A, LeMeur M, Piazza PV, Borrelli E. Distinct functions of the two isoforms of dopamine D2 receptors. Nature. 2000; 408:199–203. [PubMed: 11089973]

Wang H, Pickel VM. Dopamine D2 receptors are present in prefrontal cortical afferents and their targets in patches of the rat caudate-putamen nucleus. The Journal of Comparative Neurology. 2002; 442:392–404. [PubMed: 11793342]

Wang X, Schwarz TL. The mechanism of Ca2+-dependent regulation of kinesin-mediated mitochondrial motility. Cell. 2009; 136:163–174. [PubMed: 19135897]

Wang Y, Goldman-Rakic PS. D2 receptor regulation of synaptic burst firing in prefrontal cortical pyramidal neurons. Proc Natl Acad Sci USA. 2004; 101:5093–5098. [PubMed: 15051874]

Zaitsev AV, Gonzalez-Burgos G, Povysheva NV, Kroner S, Lewis DA, Krimer LS. Localization of calcium-binding proteins in physiologically and morphologically characterized interneurons of monkey dorsolateral prefrontal cortex. Cerebral Cortex. 2005; 15:1178–1186. [PubMed: 15590911]

Zimmer A, Zimmer AM, Hohmann AG, Herkenham M, Bonner TI. Increased mortality, hypoactivity, and hypoalgesia in cannabinoid CB1 receptor knockout mice. Proc Natl Acad Sci USA. 1999; 96:5780–5785. [PubMed: 10318961]

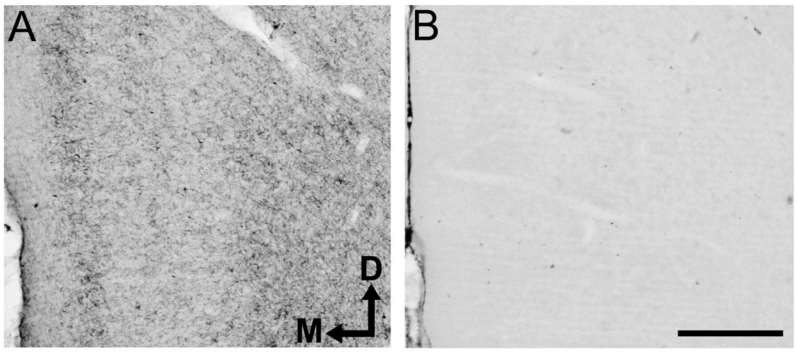

Figure 1.

CB1R immunoperoxidase is present in **(A)** wild-type mouse cingulate cortex but not **(B)** in CB1−/− cortex, confirming antibody specificity. The compass in (**A**) indicates orientation of both micrographs: **D**orsal and **M**edial. Scale bar = 200 μm.

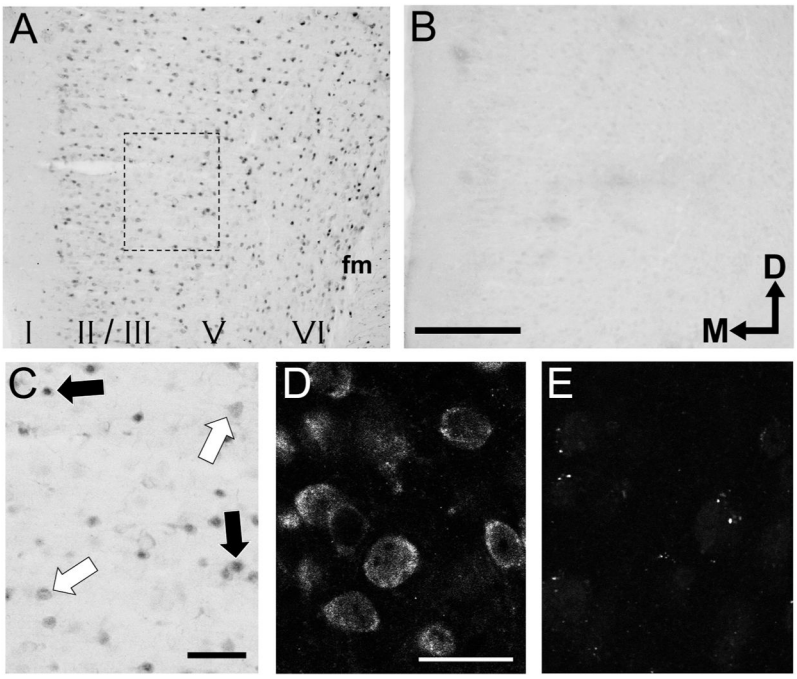

Figure 2.

Photomicrographs of sections through the mouse PL showing immunoperoxidase labeling with **(A)** the D2R antiserum and **(B)** with adsorption control, which completely blocks labeling. Labeled cell bodies are seen in layers II through VI, as indicated. The compass in **(B)** indicates orientation of all micrographs: **D**orsal and **M**edial. Scale bar = 200 μm, **fm** = forceps minor. Panel **(C)** is an enlargement of the rectangle outlined by the dotted line in **(A)**. In this area of relatively sparse labeling, black arrows indicate somata that are intensely labeled for the D2R, while white arrows indicate more lightly labeled cell bodies. Scale bar = 50 μm. Immunofluorescent labeling with the D2R is shown in **(D)**, while the immunofluorescent adsorption control is shown in **(E)**. Scale bar in **(D)** = 25 μm.

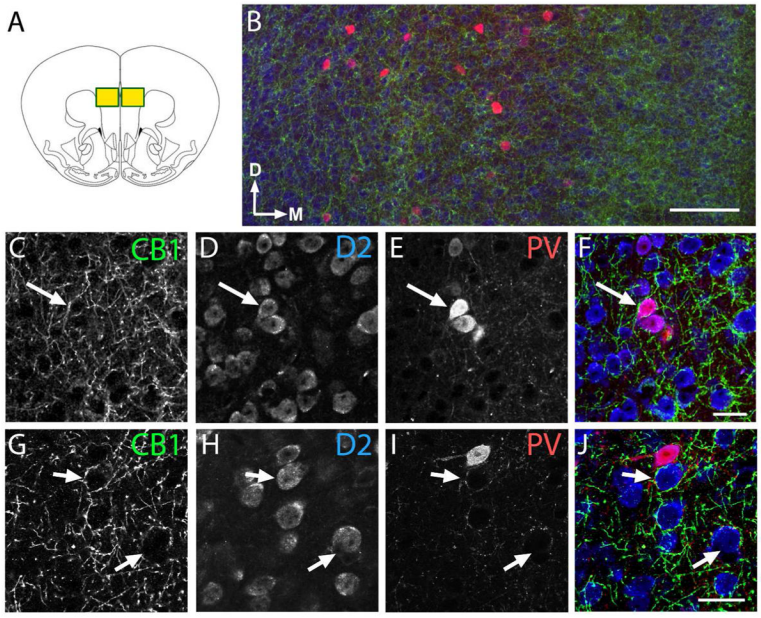

Figure 3.

Confocal micrographs showing immunoreactivity for the CB1R, D2R, and parvalbumin in the prelimbic prefrontal cortex (PL) of WT mice. **(A)** The PL area sampled (yellow boxes) is illustrated in a coronal section through the mouse forebrain at 1.94 mm to Bregma (graphically adapted from Paxinos and Franklin, 2001). **(B)** A low magnification photomicrograph shows the laminar distribution of the CB1R (represented on the green channel), parvalbumin (on the red channel), and the D2R (on the blue channel). Scale bar = 100 μm. The compass indicates orientation of this and all subsequent micrographs in the panel: **D**orsal and **M**edial. **(C–F)** Parvalbumin-immunoreactive interneurons are occasionally contacted by axonal varicosities expressing the CB1R. The white arrow indicates a soma dual-labeled for the D2R and parvalbumin that is surrounded by basket-like CB1R-immunoreactive axonal processes. All parvalbumin-positive interneurons within this field co-express the D2R. Scale bar = 25 μm. **(G–J)** Parvalbumin and CB1R-immunoreactive processes frequently contact the same neuron. White arrows indicate two somata single-labeled for the D2R that are contacted by CB1R and parvalbumin axonal processes. Scale bar = 25 μm.

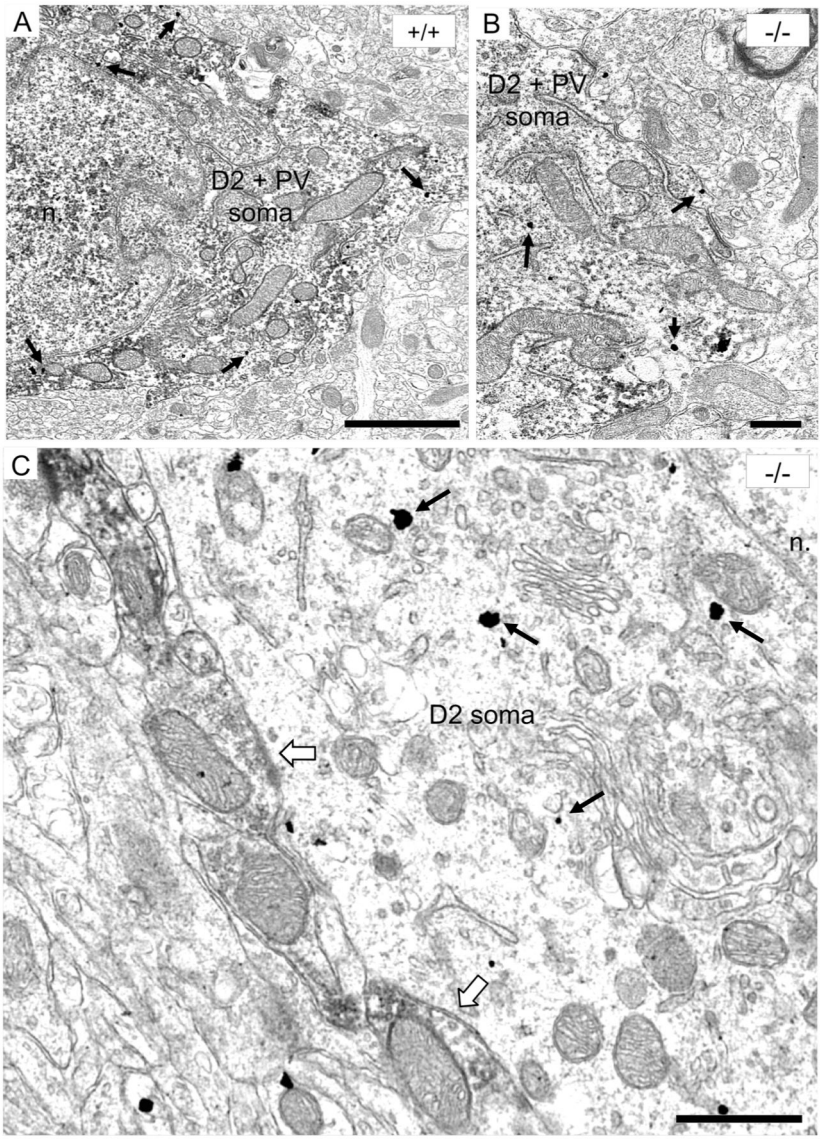

Figure 4.

Electron micrographs, all of which are taken from the mouse PL, show neuronal somatas labeled for parvalbumin (immunoperoxidase) and the D2R (immunogold, indicated by black arrows). Genotype is specified in the upper right hand corner of each panel. **(A, B)** The D2R is localized to the plasmalemma or endomembranes within the cytoplasm of parvalbumin-containing somata, which are characterized by an abundance of mitochondria. The invaginated nuclear membrane is typical of fast-firing interneurons. The D2R is localized to the plasmalemma or endomembranes within the cytoplasm. Scale bar = 2 μm in **A** and 500 nm in **B. (C)** A large D2R immunoreactive soma is contacted by parvalbumin terminals, as indicated by white arrows. The D2R-containing somatic profile in this micrograph is likely to be from a pyramidal neuron, as it is large in size, contacted by multiple inhibitory-type axon terminals, and contains stacked Golgi (Peters *et al.*, 1991). Scale bar = 500 nm, D2 = D2R, PV = parvalbumin, n. = nucleus.

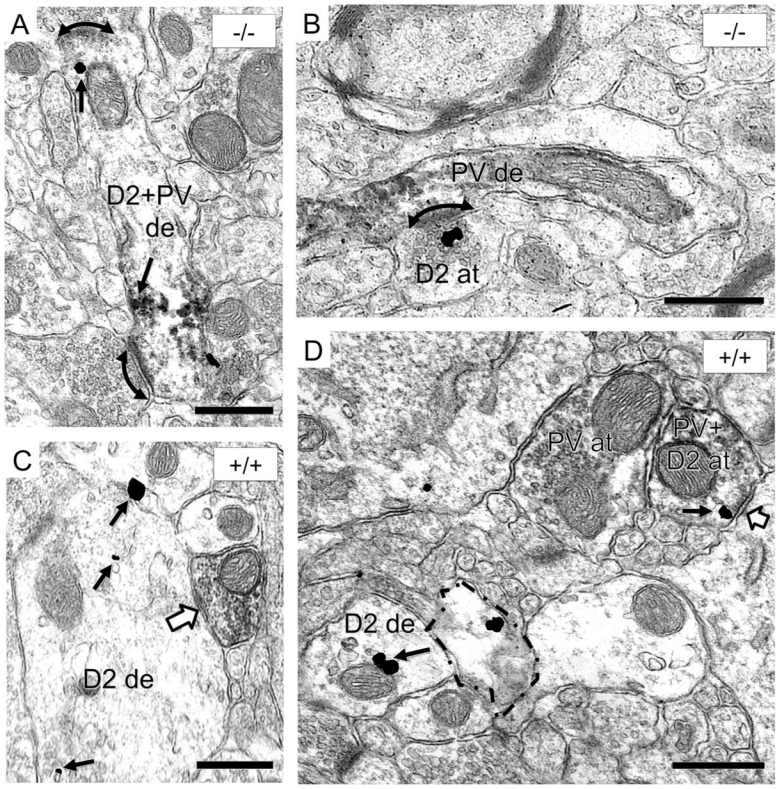

Figure 5.

Pre-synaptic axonal and post-synaptic dendritic distribution of parvalbumin and the D2R identified respectively by immunoperoxidase and immunogold labeling. **(A)** A longitudinally sectioned dendritic shaft containing parvalbumin and D2R-immunogold (black arrows) is contacted by two asymmetric excitatory-type terminals (curved arrows). **(B)** A parvalbumin-immunoreactive dendritic shaft (PV-de) receives an asymmetric synapse (curved arrow) from a D2R-labeled axon terminal (D2 at). **(C)** A D2R-labeled (black arrow) dendrite (D2 de) receives a symmetric inhibitory-type synapse (white arrow) from a parvalbumin-immunoreactive terminal. **(D)** A dual-labeled axon terminal (D2+PV at) forms a symmetric synapse with an unlabeled somatic profile (white arrow) and apposes an axon terminal labeled for parvalbumin but not the D2R. In the lower left, two D2R-immunogold particles are in contact with a mitochondrion in a small dendrite (D2 de). A neighboring glial profile (outlined in the dotted line) also contains D2R immunogold particles. Scale bars = 500 nm, de = dendrite, PV = parvalbumin, D2 = D2R, at = axon terminal.

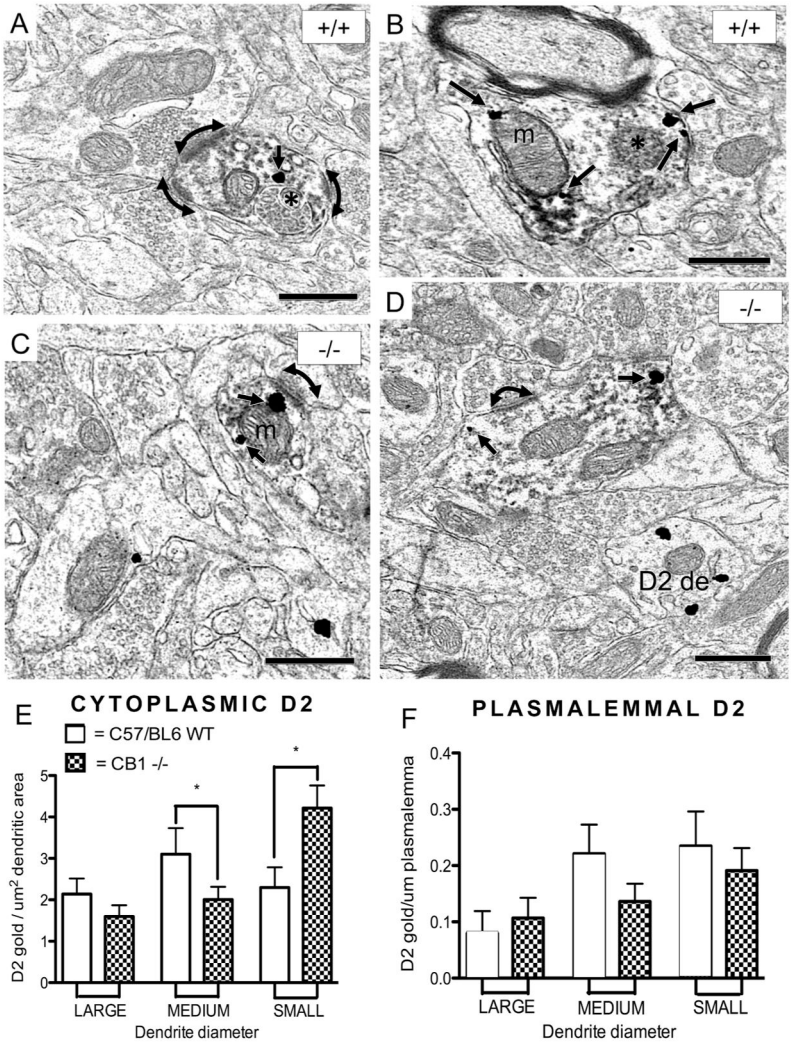

Figure 6.

Altered compartmentalization of the D2R immunogold in dendrites containing immunoperoxidase labeling for parvalbumin in the PL of the CB1−/− mice. **(A)** A small dually labeled dendritic profile from a wild-type mouse receives multiple excitatory-type terminals (curved arrows) from unlabeled terminals. The single D2R immunogold particle (arrow) is located near a multivesicular body (*). **(B)** A medium-sized parvalbumin-labeled dendritic profile from a CB1+/+ mouse contains four D2R immunogold particles (arrows), two of which are located on or near the plasma membrane contacted by an unlabeled terminal. These particles are near a multivesicular body (*), whereas other D2R immunogold particles and much of the parvalbumin immunoreactivity is affiliated with outer mitochondrial membranes and associated endoplasmic reticulum (not labeled in figure). **(C)** A small parvalbumin-labeled dendritic profile from a CB1−/− mouse contains two D2R immunogold particles and is receptive to a terminal forming an asymmetric, excitatory-type synapse. **(D)** A medium-sized dual-labeled dendritic profile from a CB1−/− mouse contains two immunogold particles. **(E)** Cluster analysis reveals a significant change in compartmental distribution of D2R immunogold in parvalbumin dendrites of CB1−/− mice. D2R immunogold density was assessed as particles of D2R immunogold/square μm dendritic area. In CB1−/− mice relative to CB1+/+ controls, a significant ($p<0.05$) increase in D2R immunogold was observed in small dendrites, while a decrease in D2R immunogold

per μm dendritic area was observed in medium parvalbumin dendrites in CB1−/− mice relative to controls. Error bars represent standard error throughout. **(F)** No significant changes in plasmalemmal distribution (measured as D2R immunogold/μm plasmalemma) were observed between groups in any dendritic compartments. Scale bars = 500 nm, de = dendrite, m = mitochondrion, * = multivesicular body.

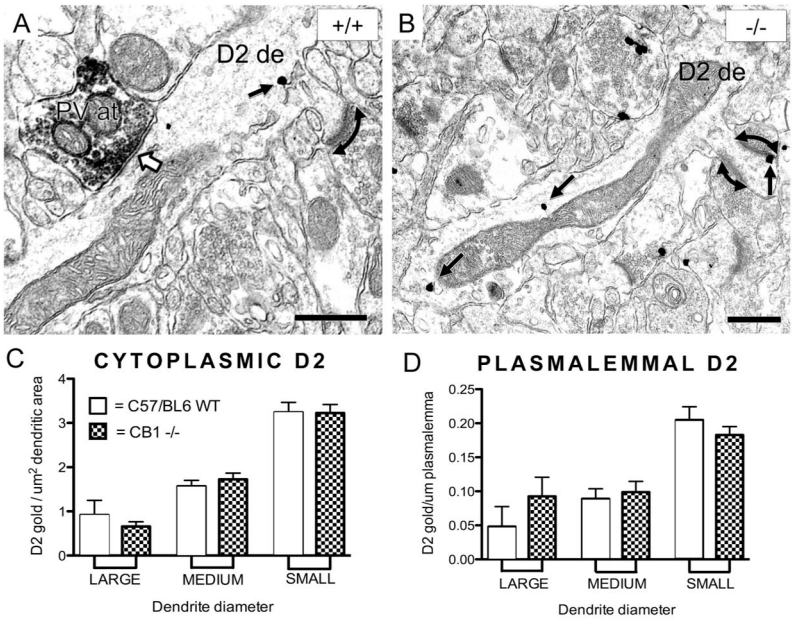

Figure 7.

Lack of CB1R genotype-specific differences in D2R immunogold labeling in PL dendrites that do not express parvalbumin. **(A, B)** Electron micrographs show no qualitative differences between CB1+/+ and CB1−/− mice in D2R-immunogold in dendritic profiles without detectable peroxidase labeling for parvalbumin. In **A**, the D2R-labeled dendrite (D2 de) receives a symmetric inhibitory-type contact (white arrow) from an axon terminal containing parvalbumin immunoperoxidase labeling (PV at). A dendritic spine protruding from the shaft receives an asymmetric excitatory-type synapse (curved arrow) from an unlabeled axon terminal. In **B,** D2R immunogold (black straight arrows) is contained within the dendritic shaft as well as on the synaptic density of a spine protrusion receptive to two asymmetric excitatory-type inputs (curved arrows). **(C, D)** Bar graphs showing no significant genotype-specific differences in either the cytoplasmic or plasmalemmal D2R immunogold density in large, medium, or small dendritic profiles. Scale bars = 500 nm, de = dendrite.

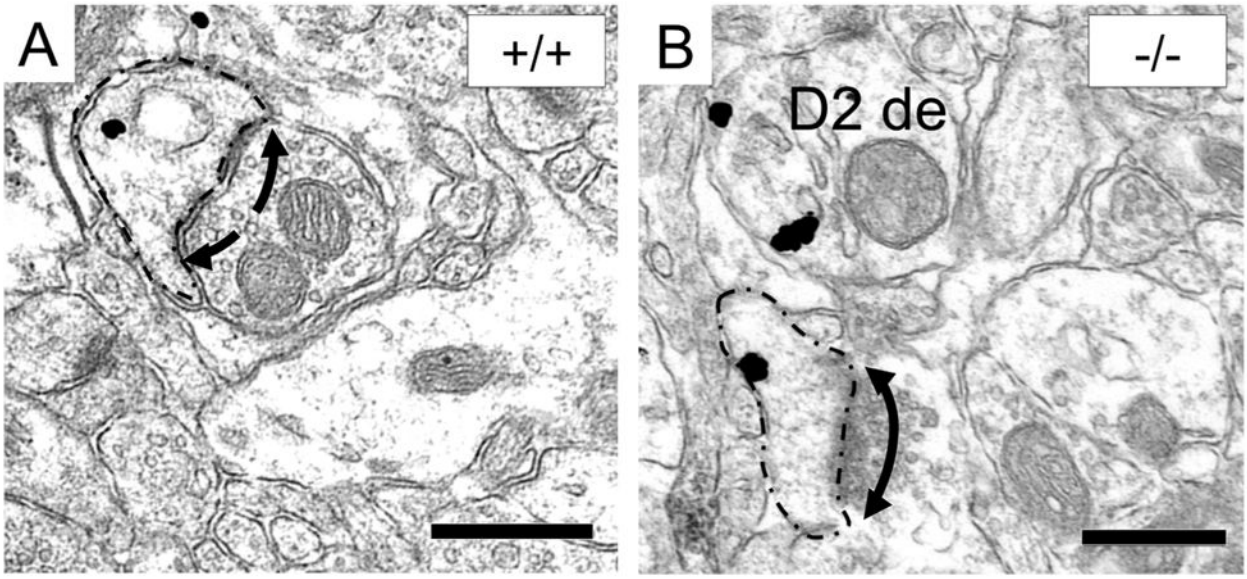

Figure 8.

Equivalent D2R immunogold labeling in dendritic spines within the PL of CB1+/+ and CB1−/− mice. **(A)** D2R immunogold is contained within the cytoplasm of a dendritic spine (outlined in a dotted line) that receives a perforated synapse (broken arrow) from an unlabeled axon terminal. **(B)** A single D2R immunogold particle is located on the plasmalemmal membrane of a dendritic spine that receives an asymmetric synaptic contact with a small, unlabeled terminal. Scale bars = 500 nm, de = dendrite.

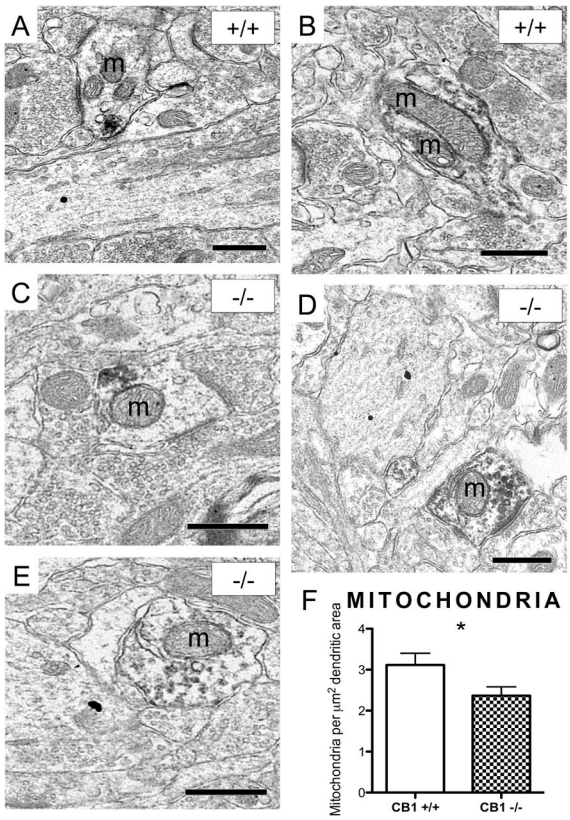

Figure 9.

Reduction in mitochondrial number in dendrites of parvalbumin-labeled interneurons in the PL of CB1−/− mice relative to controls. **(A, B)** Electron micrographs indicate multiple mitochondria within dendritic profiles labeled for parvalbumin in the CB1+/+ PL. **(C–E)** Electron micrographs showing single mitochondria within parvalbumin-positive dendritic profiles of the CB1−/− PL. **(F)** Quantification reveals a significant decrease in the number of mitochondria per square μm dendritic area in dendritic profiles of CB1−/− mice with visible parvalbumin.

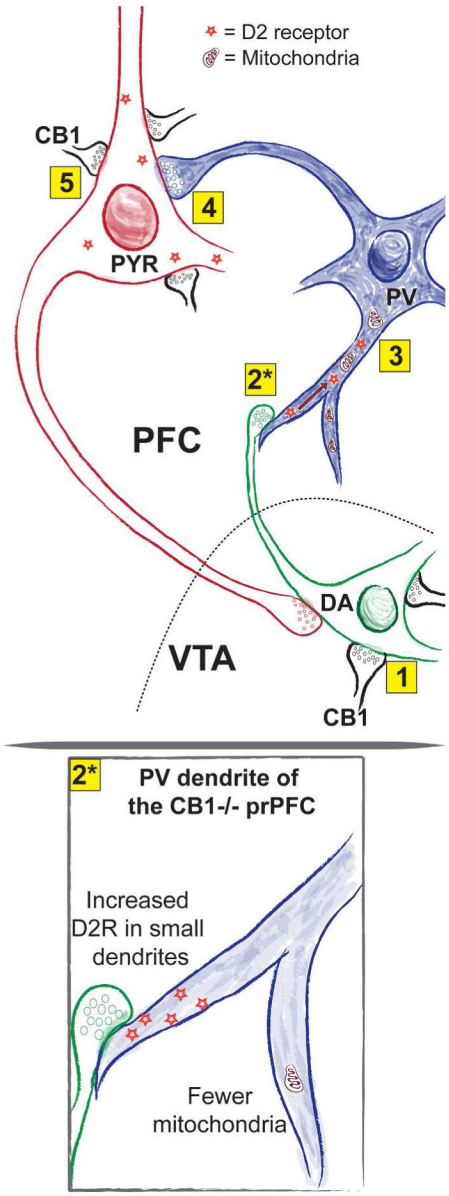

Figure 10.

A schematic diagram illustrating our observations within the context of the known mesolimbic dopaminergic circuitry influenced by cannabinoids. **1.** Dopaminergic input to the PFC originates in projection neurons of the VTA. These dopamine (DA) neurons are modulated by GABAergic as well as some glutamatergic axon terminals that express the CB1R. The dopaminergic outflow of these cells, therefore, is likely to be altered in CB1−/− mice. **2.** A number of dopaminergic axon terminals from the VTA target dendrites of parvalbumin interneurons in the PFC. These parvalbumin interneurons frequently express the D2R (orange stars) and **(3)** an abundance of mitochondria. **2*.** In parvalbumin dendrites of CB1−/− mice, increased D2R was observed in smaller, more distal processes while less D2R was observed in medium-sized dendrites, indicative of a D2R trafficking deficit. Furthermore, parvalbumin immunoreactivity is decreased in the CB1−/− PL (illustrated here as a lighter shade) and fewer mitochondria are observed in dendrites of these interneurons. **4.** The synaptic output of parvalbumin interneurons most frequently inhibits somatodendritic

processes of pyramidal neurons, some of which express the D2R. The inhibitory output of parvalbumin interneurons may also be decreased in CB1−/− mice. **5.** These same pyramidal neurons are also receptive to input from CB1R-containing GABAergic axon terminals, which is likely to be increased in mice lacking the CB1R. Finally, these pyramidal neurons project back to impinge upon dopaminergic projection neurons of the VTA.

Table 1

List of primary antibodies.

Antigen	Immunogen	Antibody Description	Source	Dilutions (IFC, immunogold, immunoperoxidase)
Parvalbumin	Frog muscle parvalbumin	Mouse monoclonal	Sigma-Aldrich (St. Louis), #P3088	1:3000, N/A, 1:3000
Dopamine D2 receptor	Amino acids 216–311 of the human D2R long isoform	Rabbit polyclonal	Laboratory of Dr. Ken Mackie, Indiana University Purification date: 2/5/08 (Kearn et al., 2005)	1:500, 1:350, 1:500
Cannabinoid CB1 receptor	The C-terminus (the last 73 amino acid residues) of the rat CB1 receptor.	Guinea pig polyclonal	Laboratory of Dr. Ken Mackie, Indiana University Purification date: 2/18/10 (Katona et al., 2006)	1:2000, N/A, 1:2000

Table 2

Comparison of the relative (%) distribution of neuronal profiles labeled for the D2R (D2), parvalbumin (PV) or both (D2 + PV) in the PL of the 4 CB1−/− and 6 CB1+/+ mice examined. No significant between-genotype differences are seen by chi-squared analysis (λ^2=7.062, 8 d.f., p = 0.53).

	D2 dendrite	D2 + PV dendrite	PV dendrite	D2 spine	D2 axon or terminal	D2 + PV axon or terminal	PV axon or terminal	PV spine	Myelinated PV axon
CB1 +/+	35%	7%	12%	5%	23%	3%	13%	1%	1%
CB1 −/−	34%	7%	15%	7%	23%	2%	9%	2%	1%